

## Electronic Supplementary Information

Mapping the Electrogenerated Chemiluminescence Reactivity in Space: Mechanistic Insight  
into Model Systems Used in Immunoassays

Milica Sentic,<sup>a,b</sup> Milena Milutinovic,<sup>a,b</sup> Frédéric Kanoufi,<sup>c</sup> Dragan Manojlovic,<sup>b</sup> Stéphane Arbault<sup>a</sup> and Neso Sojic<sup>a</sup>

<sup>a</sup> University of Bordeaux, Institut des Sciences Moléculaires, CNRS UMR 5255, ENSCBP,  
33607 Pessac, France

<sup>b</sup> Faculty of Chemistry, University of Belgrade, 11000 Belgrade, Serbia

<sup>c</sup> ESPCI ParisTech, PECSA, CNRS UMR 7195, 75231 Paris Cedex 5, France

### 1. Materials.

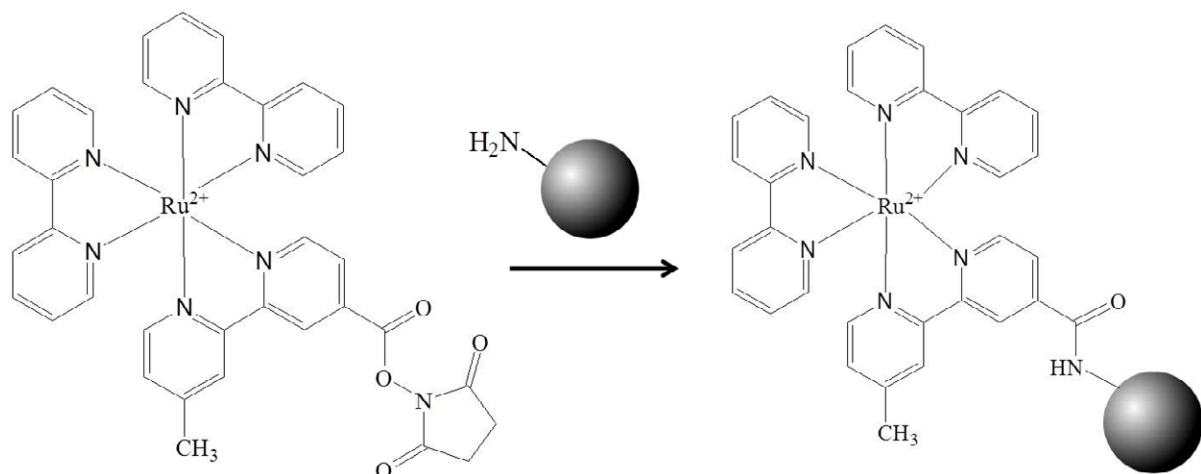
All the reagents were purchased from Sigma-Aldrich unless otherwise noted. Solutions were prepared daily using Milli-Q water (resistivity = 18 MΩ cm). Tri-*n*-propylamine (TPrA) was dissolved in PBS by addition of H<sub>3</sub>PO<sub>4</sub> (to adjust the pH to 7.4) and deaerated with Ar for 30 min.<sup>1</sup> Capture antibody specific for interleukin 8 (IL-8), the complementary biotinylated detection antibody and IL-8 recombinant protein were obtained from R&D Systems, Inc. (Minneapolis, MN). The streptavidin-modified ruthenium complex used as a label in the immunoassay experiments was synthesized according to the procedure described by Deiss et al.<sup>2</sup> Polystyrene (PS) beads were purchased from Kisker Biotech GmbH & Co.

### Immunoassay with 3-μm diameter PS beads

Antigen storage aliquots were prepared in PBS 1x/BSA 0.1% and detection antibody storage aliquots were prepared in tris-buffered saline (TBS StartingBlock). Each washing step was done in 100 μL of TBS with 1% Tween 20. The assay was performed by incubating for 2 hours the microbeads functionalized with a capture antibody (anti-IL-8) first in a sample containing antigen (dilute to the appropriate concentration with PBS StartingBlock) and washed. Then they were incubated for 30 min. in 50 μL of the detection antibodies solution (3μg/mL of antibody in PBS StartingBlock) and washed. Beads were then incubated in a solution of biotinylated detection antibody and washed again. Finally, the ECL label was attached to formed immunocomplex by exposing the beads to a solution containing a streptavidin-modified Ru(bpy)<sub>3</sub><sup>2+</sup> complex. Beads were then washed for the last time and immobilized on the electrode surface for ECL imaging.

## Functionalization of the 12- $\mu$ m diameter beads with the ruthenium label

The surface of the PS beads beared -NH<sub>2</sub> groups which allow further functionalization with the ruthenium label. 10  $\mu$ L of beads suspension (2.5%) was washed with PBS, pH=7.4 and re-suspended in 1 mL of PBS. In the same time, 1 mg of Ru(bpy)<sub>3</sub><sup>2+</sup>-NHS ester (bis(2,2'-bipyridine)-4'-methyl-4-carboxybipyridine-ruthenium N-succinimidyl ester-bis(hexafluorophosphate) was dissolved in 100  $\mu$ L of dimethyl sulfoxide and this solution was added to the beads suspension. This mixture was incubated on +4°C for 3 hours with continuous stirring. After the incubation the beads were washed from reaction solution with PBS 10-15 times by the centrifugation for 10 min at 10000 rpm to separate the beads from the solution. Finally, beads were suspended in 1 mL PBS and kept at 4°C.



Scheme S1. Functionalization of the bead with Ru(bpy)<sub>3</sub><sup>2+</sup>-based complex *via* the peptide coupling.

## 2. Instrumentation.

For the electrochemical set-up, the working electrode were glassy carbon (GC) or Au electrodes, the counter electrode a platinum wire. All the experiments were performed with a  $\mu$ Autolab type III potentiostat using an Ag/AgCl/KCl(3M) electrode as the reference electrode.

The instrument used for PL and ECL imaging was a modified epifluorescence microscope (BX-30, Olympus) similar to the one described previously.<sup>3</sup> PL and ECL emission was collected by a 50x microscope objective and detected by an Electron Multiplying Charge Coupled Device (EM-CCD) Camera (Hamamatsu, 9100-13)

### 3. ECL signals recorded in the top-view configuration

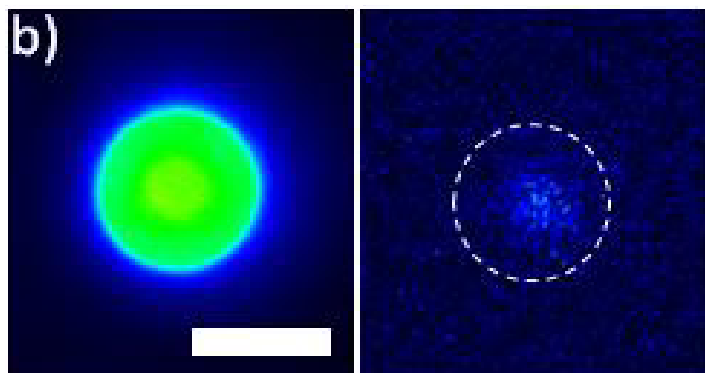
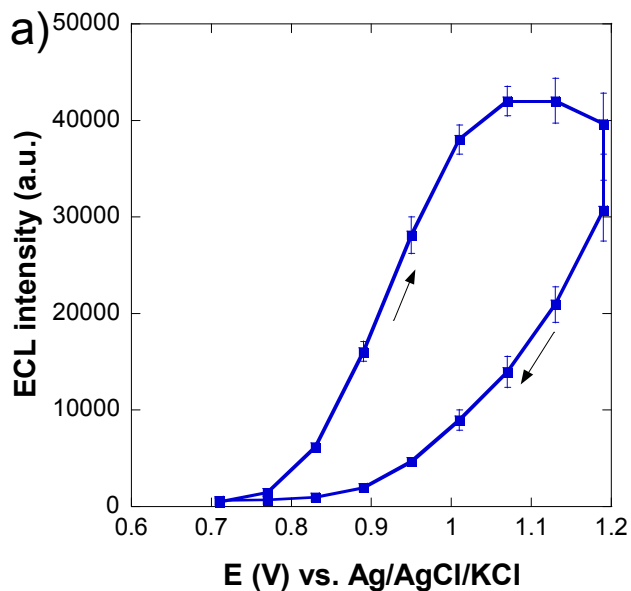


Figure S1. a) ECL intensity measured on a PS bead as a function of the potential applied to the GC electrode in a PBS solution containing 100 mM TPrA (pH = 7.4). b) Top-view PL (left) and ECL (right) images of a 12- $\mu\text{m}$  PS bead functionalized with the ruthenium label. ECL image was recorded over a 6 s exposure-time at 1.2 V in a PBS (pH = 7.4) solution containing 20 mM DBAE on Au electrode. The dashed line materializes the position of the bead. Scale bar: 10  $\mu\text{m}$ .

#### 4. PL and ECL signals recorded in the side-view configuration.

##### TPrA<sup>•+</sup> radical half-life time

The signature of the TPrA<sup>•+</sup> lifetime is obtained with a single ECL image from the distribution of the light intensity. A value of  $2920\text{ s}^{-1}$  is extracted from the ECL profile for the rate constant  $k_3$  of the TPrA<sup>•+</sup> deprotonation (reaction 3). Assuming that this reaction is a first-order process, the half-life time ( $\tau_{1/2}$ ) is  $\tau_{1/2} = \ln 2 / k_3$ . It gives a value of  $\sim 0.24\text{ ms}$ .

##### ECL with DBAE on Au electrode

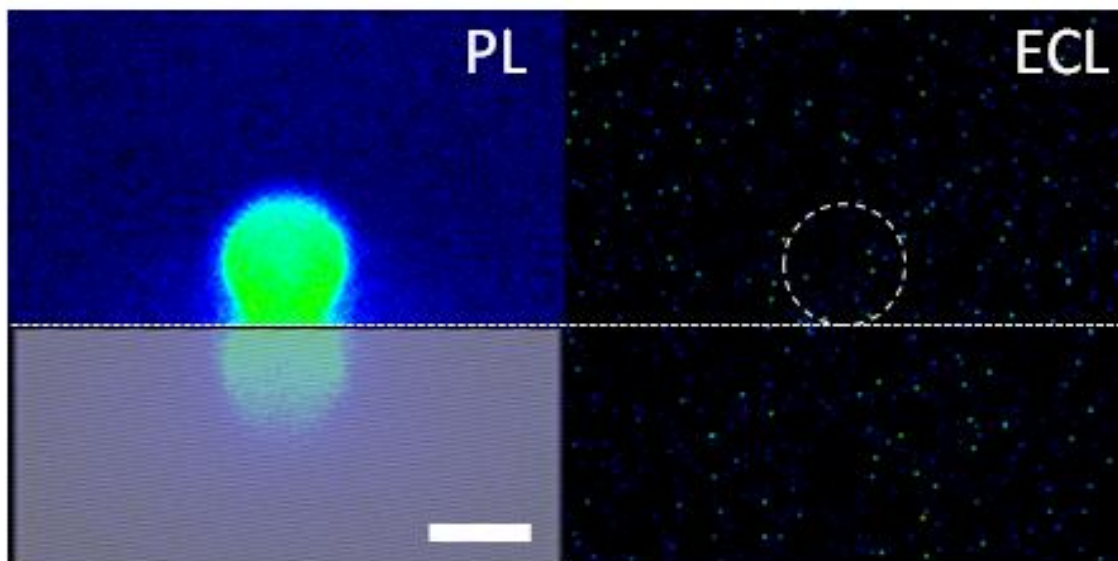


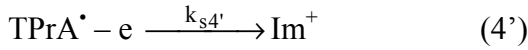
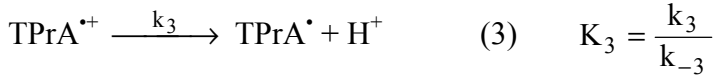
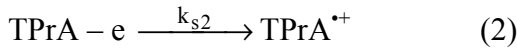
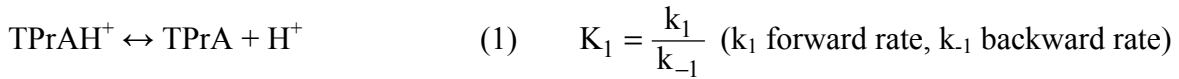
Figure S2. Side-view PL (left) and ECL (right) images of 12- $\mu\text{m}$  PS beads functionalized with the ruthenium label. ECL image was recorded over a 20 s exposure-time at 1.2 V in a PBS (pH = 7.4) solution containing 20 mM DBAE on Au electrode. The dashed line materializes the position of the bead on the electrode surface (*i.e.*  $z = 0$ ) which is represented by the dotted line. The hatched zone represents the reflection of the PL on the electrode surface. Same experimental conditions as in Figure 1. Scale bar: 10  $\mu\text{m}$ .

#### 5. Simulations.

##### Presentation

The experimental configuration was modeled using the commercial Comsol Multiphysics finite element software (version 3.4). The 2D axysymmetric geometry used is schematized in Figure S5. The cell is taken as 60  $\mu\text{m}$  large (also the size of the electrode) and 6 mm high for a bead of radius 6  $\mu\text{m}$ . The kinetic and thermodynamic parameters were the values suggested by Miao et al,<sup>4</sup> except for the TPrA<sup>•+</sup> cleavage rate constant which was chosen as an

adjustable parameter (see Figure S4). The proposed model accounts for diffusion/reaction in solution of TPrA (in its neutral and protonated form  $\text{TPrAH}^+$ ), its radical cation,  $\text{TPrA}^{\bullet+}$ , the radical issuing from  $\text{TPrA}^{\bullet+}$  deprotonation,  $\text{TPrA}^{\bullet}$ , the iminium product,  $\text{Im}^+$ , and of a pH buffer,  $\text{BufH}^+/\text{Buf}$  in excess for negligible variation of the  $\text{H}^+$  content during the ECL experiment. The boundary conditions imposed at the electrode surface correspond to the oxidation both of TPrA (generation of  $\text{TPrA}^{\bullet+}$ ) and of the radical  $\text{TPrA}^{\bullet}$  (generation of  $\text{Im}^+$ ). The upper solution boundary correspond to initial concentrations and the right boundary to no flux so that to produce preferential diffusion along the  $z$  axis. The oxidation rates are modeled by Butler-Volmer laws with sufficiently fast rate so that the oxidation proceeds under diffusion control. The solution diffusion equations and boundaries at the electrode are given accordingly to the different chemical reactions, diffusion/reaction equations ( $\Delta$  is the Laplacian in 2D axisymmetric geometry) and electrode transformation fluxes:



$$\frac{\partial[\text{TPrA}]}{\partial t} = D_{\text{sol}} \Delta[\text{TPrA}] - k_1[\text{BufH}^+] [\text{TPrA}] + k_{-1}[\text{Buf}] [\text{TPrAH}^+] \quad (\text{S.1})$$

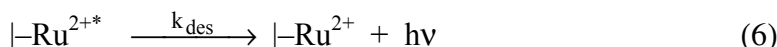
$$\frac{\partial[\text{TPrA}^{\bullet+}]}{\partial t} = D_{\text{sol}} \Delta[\text{TPrA}^{\bullet+}] - k_3[\text{TPrA}^{\bullet+}] \quad (\text{S.2})$$

$$\frac{\partial[\text{TPrA}^{\bullet}]}{\partial t} = D_{\text{sol}} \Delta[\text{TPrA}^{\bullet}] + k_3[\text{TPrA}^{\bullet+}] \quad (\text{S.3})$$

$$D_{\text{sol}} \left. \frac{\partial[\text{TPrA}]}{\partial r} \right|_{\text{el,surf}} = -D_{\text{sol}} \left. \frac{\partial[\text{TPrA}^{\bullet+}]}{\partial r} \right|_{\text{el,surf}} = -k_{s1}[\text{TPrA}] \quad (\text{S.4})$$

$$D_{\text{sol}} \left. \frac{\partial[\text{TPrA}^{\bullet}]}{\partial r} \right|_{\text{el,surf}} = -D_{\text{sol}} \left. \frac{\partial[\text{Im}^+]}{\partial r} \right|_{\text{el,surf}} = -k_{s4'}[\text{TPrA}^{\bullet}] \quad (\text{S.5})$$

The ECL emission requires the modeling of the reaction of the radical intermediates generated in solution with ruthenium species immobilized at the bead surface. The model accounts for the surface concentration of  $\text{Ru}^{2+}$ ,  $\text{Ru}^+$ ,  $\text{Ru}^{2+*}$  species based on the following surface reactions with corresponding reaction rates and flux conditions at the bead surface:



$$\frac{\partial \Gamma_{\text{Ru}^{2+}}}{\partial t} = D_{\text{app,surf}} \Delta \Gamma_{\text{Ru}^{2+}} - k_4 \Gamma_{\text{Ru}^{2+}} [\text{TPrA}^\bullet] + k_{\text{des}} \Gamma_{\text{Ru}^{2+*}} \quad (\text{S.6})$$

$$\frac{\partial \Gamma_{\text{Ru}^+}}{\partial t} = D_{\text{app,surf}} \Delta \Gamma_{\text{Ru}^+} + k_4 \Gamma_{\text{Ru}^+} [\text{TPrA}^\bullet] - k_5 \Gamma_{\text{Ru}^+} [\text{TPrA}^+] \quad (\text{S.7})$$

$$\frac{\partial \Gamma_{\text{Ru}^{2+*}}}{\partial t} = D_{\text{app,surf}} \Delta \Gamma_{\text{Ru}^{2+*}} + k_5 \Gamma_{\text{Ru}^+} [\text{TPrA}^+] - k_{\text{des}} \Gamma_{\text{Ru}^{2+*}} \quad (\text{S.8})$$

$$D_{\text{sol}} \frac{\partial [\text{TPrA}^+]}{\partial r} \Big|_{\text{b,surf}} = -D_{\text{sol}} \frac{\partial [\text{TPrA}]}{\partial r} \Big|_{\text{b,surf}} = -k_5 \Gamma_{\text{Ru}^+} [\text{TPrA}^+] \quad (\text{S.9})$$

$$D_{\text{sol}} \frac{\partial [\text{TPrA}^\bullet]}{\partial r} \Big|_{\text{b,surf}} = -D_{\text{sol}} \frac{\partial [\text{Im}^+]}{\partial r} \Big|_{\text{b,surf}} = -k_4 \Gamma_{\text{Ru}^{2+}} [\text{TPrA}^\bullet] \quad (\text{S.10})$$

The ECL emission is calculated as the rate of photon emitted by any point of the surface at any computation time:

$$I_{\text{light}} \propto \frac{\partial h\nu}{\partial t} = k_{\text{des}} \Gamma_{\text{Ru}^{2+*}} \quad (\text{S.11})$$

The possibility of lateral charge transfer propagation (electron hopping) was modeled by considering apparent surface diffusion,  $D_{\text{app,surf}}$ , of all the ruthenium species over the bead surface. The ECL emission is modeled as the rate of desexcitation of the  $\text{Ru}^{2+*}$  species.

The different values employed in the model were taken from literature and are summarized in Table S1. All the fast reaction rates such as the protonation of bases (1, e, a) and the surface transformation rates of Ru complexes are diffusion controlled and changing their rate do not change the result of the simulations. The Ru surface concentration was chosen higher than that of a compact monolayer coverage. The simulation is then performed under condition of kinetic control by the  $\text{TPrA}^+$  and  $\text{TPrA}^\bullet$  chemistry in solution.

Compound	Total initial concentration	Diff. coeff. D ( $\text{cm}^2/\text{s}$ )	Thermo.	Rate constants	
Buf/BufH <sup>+</sup>	0.3	$5 \cdot 10^{-6}$	$K_{\text{buf}} = 10^{-8}$	$k_b = 2 \cdot 10^3$	$k_{-b} = 3 \cdot 10^{10}$
H <sup>+</sup>	$10^{-8}$	$9.3 \cdot 10^{-5}$	$K_e = 10^{-14}$	$k_e = 2 \cdot 10^{-3}$	$k_{-e} = 3 \cdot 10^{10}$
TPrA/TPrAH <sup>+</sup>	0.01	$5 \cdot 10^{-6}$	$K_1 = 10^{-10.4}$	$k_1 = 8$	$k_{-1} = 3 \cdot 10^{10}$
TPrA/TPrA <sup>•+</sup>			$E^0 = 0.88^b$	$k_{s2} = 10$	
TPrA <sup>•+</sup>		$5 \cdot 10^{-6}$	$K_3 > 10^3$	$k_3 \text{ adjusted}$	$k_{-3} = 0.07$
TPrA <sup>•</sup>		$5 \cdot 10^{-6}$	$E^0 = -1.7^b$	$k_{s4} = 10$	
Ru <sup>2+</sup>	$10^{-9}$	$0 - 5 \cdot 10^{-7}$		$k_4 > 3 \cdot 10^5$	
Ru <sup>+</sup>		$0 - 5 \cdot 10^{-7}$		$k_5 > 3 \cdot 10^5$	
Ru <sup>2+*</sup>		$0 - 5 \cdot 10^{-7}$		$k_{\text{des}} > 3 \cdot 10^2$	

<sup>a</sup> Units: All solution concentrations are in M, surface concentrations in mol cm<sup>-2</sup>; For all reaction except i=4 and 5, K<sub>i</sub> in M, k<sub>i</sub> in s<sup>-1</sup> and k<sub>-i</sub> in M<sup>-1</sup>s<sup>-1</sup>, k<sub>s2</sub> and k<sub>s4</sub> in cm/s, k<sub>4,5</sub> in M<sup>-1</sup>s<sup>-1</sup>, k<sub>des</sub> in s<sup>-1</sup>. <sup>b</sup> not used in the simulation the values vs Ag/AgCl are given for indication based on the cited reference.<sup>4</sup>

### Discussion

The transient concentrations of the different chemical species were simulated. The discussion of the simulated results presented in Figures S3-6 correspond to the solution obtained at long time, t = 300s. First the simulation was performed in the absence of the bead in order to reproduce the concentration profiles in solution of TPrA, buffer and H<sup>+</sup> in solution in planar diffusion obtained from Digisim®. It corresponds to the situation described by Miao et al.<sup>4</sup> The Ru derivatized bead was then introduced and the simulation restarted. For fast surface transformation rates (k<sub>4</sub> and k<sub>5</sub> fast) the ECL generation should be governed by the concentration profile of TPrA radical species at the surface of the derivatized bead. This was explained and demonstrated in more details in modeling of Scanning Electrochemical Microscopy lithography experiments.<sup>5</sup>

The concentration profiles of TPrA<sup>+</sup> and TPrA<sup>•</sup> in solution or at the bead surface and the generated light intensity, I<sub>light</sub>, were simulated. Examples of distribution of solution concentration are given in Figure S5, while the concentration profile at the bead surface, projected on the z axis, are given in Figure S3 (lines). For comparison, the concentration profile along the z axis in the solution, far from the bead r > 50μm, is given in Figure S3 (symbols).

Far from the bead (Figure S3 symbols) the concentration profiles correspond to planar diffusion simulation, they are consistent with those simulated by Digisim in Miao et al.<sup>4</sup> The concentration profiles at large z (Figures 3 and S5) are identical both in the region of the bead and far from the bead where planar diffusion is effective. Smaller concentrations are observed in the region of the bead and, particularly for TPrA<sup>+</sup>, close to the electrode surface (small z) as a result of the confinement of the solution between the bead and the electrode.

Based on the set of equations given the light intensity corresponds to a process in series, the generation of Ru<sup>+</sup> and the generation of Ru<sup>2+\*</sup>, it is then, under steady-state assumption, given by the inverse of sum of the inverse rate of their formation and

$$1/I_{\text{light}} \sim 1/[TPrA^{+}] + 1/[TPrA^{\bullet}] \quad (\text{S.12})$$

Equation (S.12) roughly explains that I<sub>light</sub> follows the smallest concentration profile (TPrA<sup>•</sup> at small z; TPrA<sup>+</sup> at large z) and is maximum when both concentrations are equals.

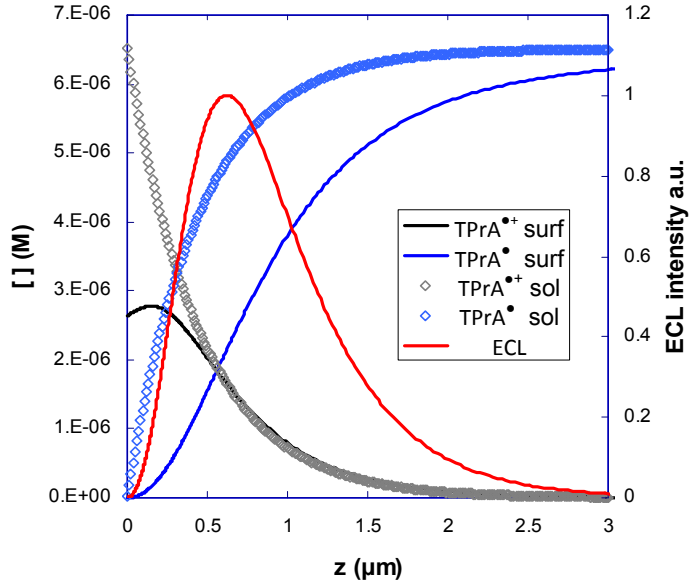


Figure S3. Concentration profiles of  $\text{TPrA}^{\bullet+}$  (black curve), of  $\text{TPrA}^\bullet$  (blue curve) and of the resulting ECL intensity (red curve) with the ruthenium complex immobilized on the bead. The depicted concentration and ECL profiles are simulated with a value of  $2920 \text{ s}^{-1}$  for the  $\text{TPrA}^{\bullet+}$  deprotonation rate constant. The concentration profiles along the  $z$  axis in the solution, i.e. far from the bead  $r > 50 \mu\text{m}$ , are depicted by the symbols.

At large  $z$ , the ECL emission is then controlled by the  $\text{TPrA}^{\bullet+}$  decay in solution and follows the shape of the reaction layer of  $\text{TPrA}^{\bullet+}$ . This reaction layer of constant thickness  $(D/k_3)^{1/2}$  does not depend on the observation time but on the lifetime of  $\text{TPrA}^{\bullet+}$  (or its decomposition rate,  $k_3$ ). This is particularly illustrated in Figure S4. The faster the decomposition rate,  $k_3$ , the smaller the reaction layer and the less expanded the region of the ECL emission. Fitting the tail of the decrease of ECL light emission (the reaction layer tail) allows a direct estimation of the radical cation decomposition rate.

In the proposed model,  $\text{TPrA}^\bullet$  is stable in solution, at least over micrometric regions or at least more stable than the cation radical  $\text{TPrA}^{\bullet+}$ . If the chemical fate of  $\text{TPrA}^\bullet$  had to be considered, it would be ruled, as discussed for  $\text{TPrA}^{\bullet+}$ , by a drop of concentration in a reaction layer of thickness dictated by its decomposition rate,  $k_{\text{rad}}$ . The tail of the  $\text{TPrA}^\bullet$  concentration profile would resemble that of  $\text{TPrA}^{\bullet+}$  but with a different length scale. When  $\text{TPrA}^\bullet$  is more stable than the radical cation  $\text{TPrA}^{\bullet+}$  ( $k_{\text{rad}} \ll k_3$ ) then (S.12) suggests the ECL profiles are not much changed compared to those simulated here, and the tail of the ECL profile is governed by  $\text{TPrA}^{\bullet+}$  lifetime. Otherwise when  $k_{\text{rad}} > k_3$  eq (S.12) suggests that the ECL profile is completely ruled by  $\text{TPrA}^\bullet$  concentration. The tail of the ECL profile is governed by  $\text{TPrA}^\bullet$  lifetime.

Fitting the tail of the decrease of ECL light emission by the same diffusion – first-order decomposition rate reaction model then provides an estimate of the apparent decomposition rate of either  $\text{TPrA}^{\bullet+}$  or  $\text{TPrA}^\bullet$  and here  $\text{TPrA}^{\bullet+}$  as considered by Miao et al.<sup>4</sup>

If the same argument and mechanism are valid for DBAE, the absence of ECL in the side view indicates the level of ECL is within noise level and about 5 times smaller than for TPrA, suggesting that the radicals of DBAE are likely  $> 10$  times less stable than  $\text{TPrA}^{\bullet+}$ .

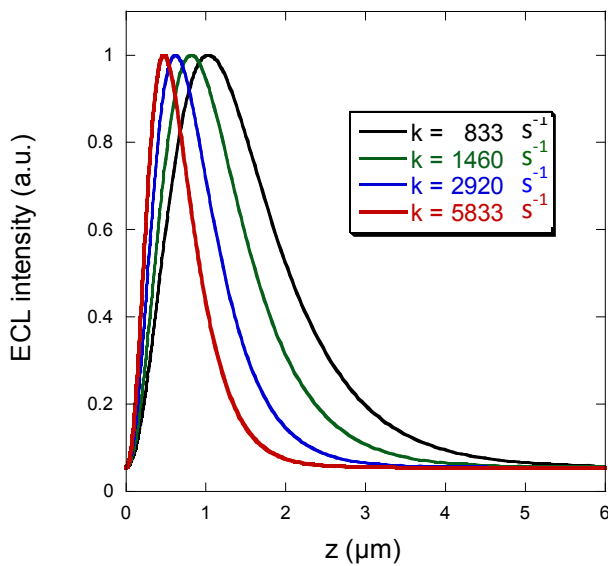


Figure S4. Effect of the kinetic rate of  $\text{TPrA}^{\bullet+}$  deprotonation on the normalized ECL intensity profile in the vicinity of a 12- $\mu\text{m}$  diameter bead.

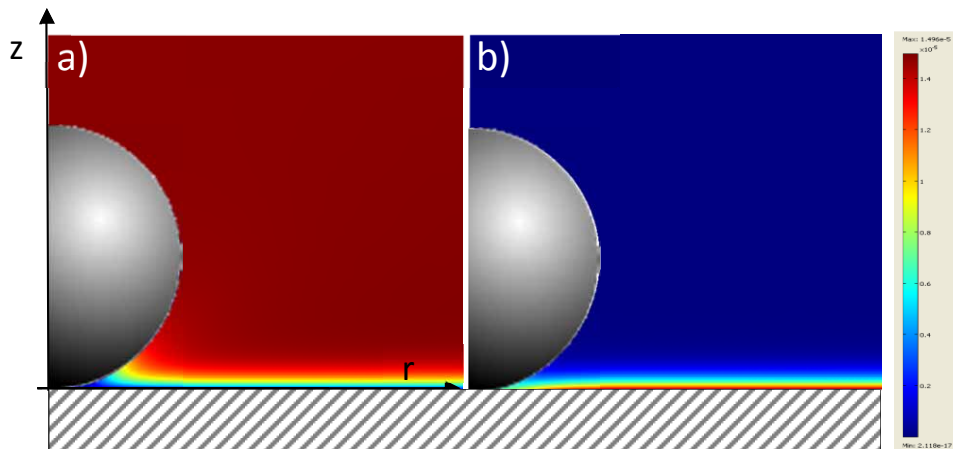


Figure S5. Simulated concentration profiles of (a)  $\text{TPrA}^{\bullet}$  and (b)  $\text{TPrA}^{\bullet+}$  in the vicinity of a 12- $\mu\text{m}$  diameter bead. The selected value for the  $\text{TPrA}^{\bullet+}$  deprotonation rate constant was  $2920 \text{ s}^{-1}$ .

Finally, electron hopping or lateral charge propagation can be implemented in the model through an apparent surface diffusion<sup>6</sup> of the Ru species,  $D_{\text{app,surf}}$ . A simulation of the ECL light emission along the bead surface when considering or not surface diffusion is presented in Figure S6. Even if surface diffusion may approach the diffusion in the condensed state (solution), usual values of apparent surface diffusion for electron-hopping can vary from 0.0001 to 0.1 times the values observed in solution.<sup>7</sup> The example of simulation proposed in

Figure S6 (right) is performed with the fastest diffusion rate  $D_{app,surf} = 0.1D_{sol}$ . If the  $I_{light}$  values are higher toward the bottom of the bead ( $z \rightarrow 0$ ), the tail of  $I_{light}$  observed at  $z > 1\mu\text{m}$  does not depend on  $D_{app,surf}$  confirming that this tail is only governed by the TPrA $^{+}$  decomposition rate.

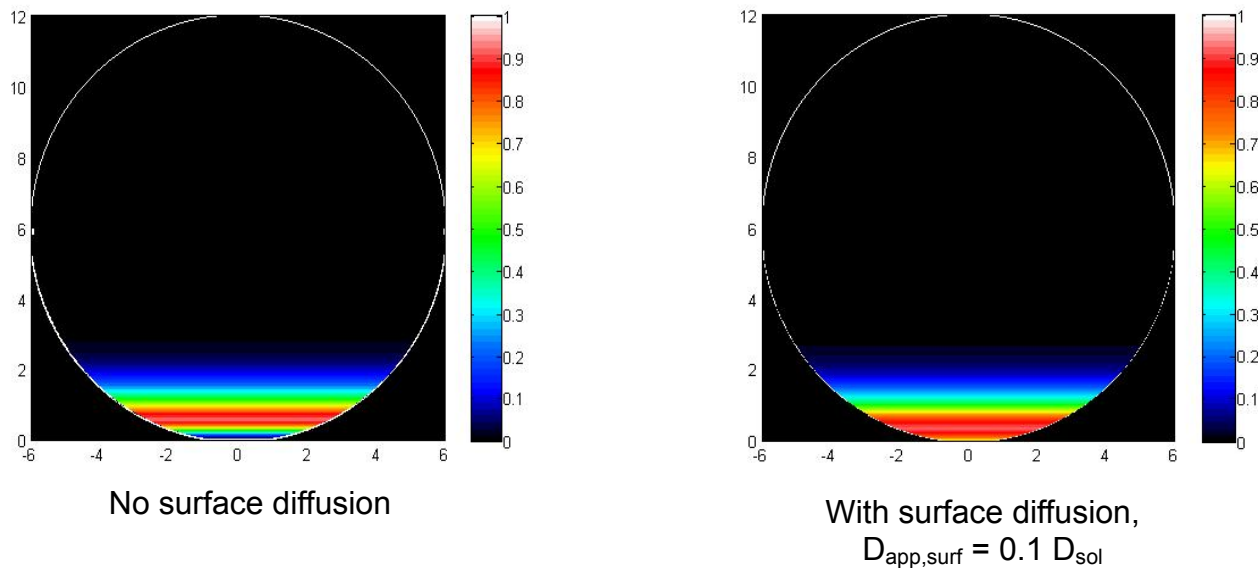


Figure S6. Effect of the electron-hopping (lateral charge propagation with apparent surface diffusion  $D_{app,surf}$ ) process on the zone of ECL production.

## References

- (1) Senthil Kumar, S.; Bard, A. J. *Anal. Chem.* **2012**, *85*, 292-295.
- (2) Deiss, F.; LaFratta, C. N.; Symer, M.; Blicharz, T. M.; Sojic, N.; Walt, D. R. *J. Am. Chem. Soc.* **2009**, *131*, 6088-6089.
- (3) Chovin, A.; Garrigue, P.; Vinatier, P.; Sojic, N. *Anal. Chem.* **2004**, *76*, 357-364.
- (4) Miao, W.; Choi, J.-P.; Bard, A. J. *J. Am. Chem. Soc.* **2002**, *124*, 14478-14485.
- (5) (a) Hazimeh, H.; Nunige, S.; Cornut, R.; Lefrou, C.; Combellas, C.; Kanoufi, F. *Anal. Chem.* **2011**, *83*, 6106-6113. (b) Nunige, S.; Cornut, R.; Hazimeh, H.; Hauquier, F.; Lefrou, C.; Combellas, C.; Kanoufi, F. *Angew. Chem. Int. Ed.* **2012**, *51*, 5208-5212.
- (6) Andrieux, C. P.; Savéant, J.-M. *J. Electroanal. Chem.* **1980**, *111*, 377-381.
- (7) (a) Amatore, C.; Bouret, Y.; Maisonhaute, E.; Goldsmith, J. I.; Abruna, H. D. *Chem. Eur. J.* **2001**, *7*, 2206-2226. (b) Lee, W.-Y.; Majda, M.; Brezesinski, G.; Wittek, M.; Möbius, D. *J. Phys. Chem. B* **1999**, *103*, 6950-6956.